MAGNETIC HELICITY BUDGET OF SOLAR-ACTIVE REGIONS FROM THE PHOTOSPHERE TO MAGNETIC CLOUDS

C.H. MANDRINI[1,*], P. DÉMOULIN[2], L. VAN DRIEL-GESZTELYI[2,3,4,5], L.M. GREEN[3] and M.C. LÓPEZ FUENTES[6]

[1]*Instituto de Astronomía y Física del Espacio, IAFE, CC. 67 Suc. 28, 1428 Buenos Aires, Argentina; E-mail: mandrini@iafe.uba.ar*

[2]*Observatoire de Paris, section Meudon, LESIA (CNRS), F-92195 Meudon Principal Cedex, France*

[3]*Mullard Space Science Laboratory, University College London, UK*

[4]*Centre for Plasma Astrophysics, K.U. Leuven, Celestijnenlaan 200B, 3001 Heverlee, Belgium*

[5]*Konkoly Observatory, Hungary*

[6]*Naval Research Laboratory, Code 7675, Washington DC 20375-5352, USA*

Abstract. We have analyzed the long-term evolution of two active regions (ARs) from their emergence through their decay using observations from several instruments on board SoHO (MDI, EIT and LASCO) and Yohkoh/SXT. We have computed the evolution of the relative coronal magnetic helicity combining data from MDI and SXT with a linear force-free model of the coronal magnetic field. Next, we have computed the injection of helicity by surface differential rotation using MDI magnetic maps. To estimate the depletion of helicity we have counted all the CMEs of which these ARs have been the source, and we have evaluated their magnetic helicity assuming a one to one correspondence with magnetic clouds with an average helicity contain. When these three values (variation of coronal magnetic helicity, injection by differential rotation and ejection via CMEs) are compared, we find that surface differential rotation is a minor contributor to the helicity budget since CMEs carry away at least 10 times more helicity than the one differential rotation can provide. Therefore, the magnetic helicity flux needed in the global balance should come from localized photospheric motions that, at least partially, reflect the emergence of twisted flux tubes.We estimate that the total helicity carried away in CMEs can be provided by the end-to-end helicity of the flux tubes forming these ARs. Therefore, we conclude that most of the helicity ejected in CMEs is generated below the photosphere and emerges with the magnetic flux.

Keywords: Sun: corona, magnetic field, coronal mass ejections (CMEs)

1. Introduction

Observational evidence of cycle-invariant hemispheric helical patterns in the solar atmosphere dates from more than 75 years. Hale (1925) observed the existence of vortices around sunspots that exhibited a preferred rotational direction in each solar hemisphere independent from the solar cycle: Around 80% of sunspot vortices showed a counter-clockwise direction in the northern hemisphere and vice versa in the southern one. The results found by Hale (1925) were confirmed by Richardson

*Member of the Carrera del Investigador Científico, CONICET, Argentina.

Astrophysics and Space Science **290:** 319–344, 2004.

(1941) who extended Hale's work to four solar cycles. These early studies were followed by the discovery of hemispheric chirality patterns independent of the solar cycle in several solar and solar-related structures: active regions, coronal loops, filaments, coronal arcades and interplanetary magnetic clouds (see van Driel-Gesztelyi et al., 2003a, and references therein). Chirality rules were derived from these observations, indicating that the Sun exhibits left-handed features in its northern hemisphere and right-handed features in the southern one.

Magnetic helicity, one of the few magnetohydrodynamic (MHD) quantities, which is preserved even under non-ideal conditions (Berger, 1984), can be used to quantify the degree of shear and/or twist in the structures mentioned above (Berger and Field, 1984; Berger, 1999). A clockwise rotation and right-handed twist of coronal loops or interplanetary flux tubes implies positive helicity, and vice versa for negative helicity. The existence of these hemispherical chirality rules, to which exceptions occur in a percentage that stays around 20–35% (see recent review by Pevtsov, and Balasubramaniam, 2003), indicates that a global underlying mechanism generating magnetic helicity with a preferred hemispheric sign should be at work in the Sun.

Combining the existence of chirality rules with the fact that magnetic helicity is a well preserved quantity, one infers that unless the Sun finds a way to shed it, magnetic helicity will accumulate in each coronal hemisphere (unless important reconnection occurs between north and south hemispheres). Rust (1994) and Low (1996) suggested that coronal mass ejections (CMEs) are the natural way through which the active region corona is able to expel the accumulated helicity. Observationally, CMEs have been linked to the ejection of helical structures from the Sun due to an instability of the coronal field (see e.g. Cliver and Hudson, 2002). The ejected plasmoid carries part of the magnetic helicity of its original source magnetic field. There is increasing observational evidence showing that the helicity sign of magnetic clouds matches that of their source region. Bothmer and Schwenn (1994), Rust (1994) and Marubashi (1997) have found a high correlation between the helicity sign in magnetic clouds and their associated erupting filaments. Yurchyshyn et al. (2001) confirmed these statistical results in two well observed cases.

Therefore, the study of the magnetic helicity balance of solar active regions, and the consequent analysis of the most probable coronal helicity sources, are useful tools to understand the characteristics of the underlying mechanism originating helicity in the Sun. Furthermore, the conservation of magnetic helicity is a key to understand the link between phenomena present in very different physical conditions, such as in the convective zone, the corona and the interplanetary medium.

In this paper, we present the results of a comprehensive observational analysis of the coronal magnetic helicity balance of two solar active regions (ARs): NOAA AR 7978 and NOAA AR 8100. These ARs were observed on the solar disk for seven and six solar rotations, respectively. Their long-term evolution has been analyzed in detail in two previous papers (AR 7978 in Démoulin et al., 2002a, and AR 8100 in Green et al., 2002). The aim of the present paper is to stress the similarities and

differences between these two regions and to put the results of these helicity studies in the same context. We start summarizing the long-term evolution of both ARs in Section 2. In Section 3.1 we review the properties of magnetic helicity and describe the sources and sinks of helicity within a given magnetic volume. The computation of the coronal magnetic helicity is presented in Section 3.2. In Section 3.3 we compute the helicity injected in the coronal field by shearing footpoint motions, in particular by surface differential rotation; while in Section 3.4 we compute the helicity lost via CMEs. The magnetic helicity budget of both ARs is discussed in Section 3.5 and we present our conclusions in Section 4.

2. The Long-Term Evolution of the ARs

2.1. AR 7978 ALONG SEVEN SOLAR ROTATIONS

Active region NOAA 7978, as identified when it first appeared on July 1996, was the only sizeable AR observed on the solar disk during the second half of 1996. First flux appearance started at S10 E31 on July 4, 1996. The AR was born in a dominantly negative polarity environment, west of a dispersed bipolar region. By July 6, 1996, the first well-formed sunspots were observed; the fast growth of the magnetic flux lasted until around July 10 (van Driel-Gesztelyi et al., 1999). There was a second episode of flux emergence in the AR that started when the AR was on the far side of the Sun and continued for a few days after the AR rotated onto the disk for the second time. We refer the reader to Figures 1 and 2 in Démoulin et al. (2002a) for magnetic maps during these two solar rotations.

The magnetic field of the AR, as observed with the Michelson Doppler Imager (MDI, Scherrer et al., 1995) on board the Solar and Heliospheric Observatory (SoHO), was clearly distinguishable from the background field for at least seven solar rotations, until January 1997. After the first two rotations the global deformation of the flux concentrations was mainly due to the effect of diffusion and differential rotation. The evolution of AR 7978 is typical for a bipolar region (see the review by van Driel-Gesztelyi, 1998). The right column in Figure 1 illustrates the long-term evolution of the photospheric field at successive central meridian passages (CMPs), while the left column shows magnetic maps rotated to the time of the following CMP map, applying differential rotation. Comparing both columns, we observe the same tilt of the magnetic inversion line implying that the global deformation of the AR was just the result of differential rotation.

We will call the region AR 7978 along all the rotations, though it was denoted as NOAA 7981 and NOAA 7986 in the second and the third rotations, respectively. After the spots disappeared (from the fourth rotation on) the region had not a NOAA number, but we will refer to it as AR 7978.

The evolution of the total magnetic flux of the AR during the emergence and six more consecutive CMPs is depicted in the top panel of Figure 2. These flux

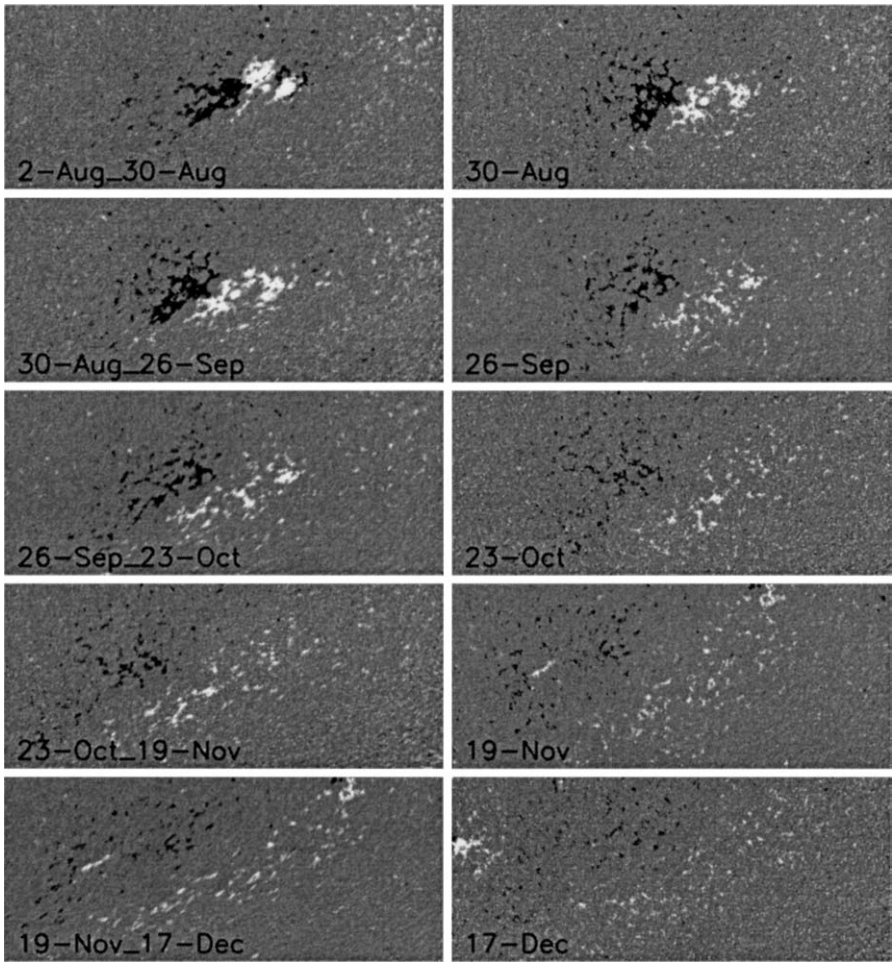

Figure 1. SoHO/MDI magnetic maps (white positive and black negative polarities) showing the long-term evolution of AR 7978 (right column). On the left column magnetograms of the right column (first date) have been transformed using the surface differential rotation profile after one solar rotation (second date). The sizes of the boxes are 650 × 325 Mm, the spatial coordinates have been corrected from projection effects. In these, as in all images, North is up and West is to the right.

measurements have been taken over a constant fixed area encompassing the AR and have been corrected because of the underestimation recently found in MDI measurements by Berger and Lites (2003). These authors found that, when compared to the Advanced Stokes Polarimeter, MDI underestimates magnetic flux densities in a factor of 0.64–0.69 for values $\leq$1200 G, which is the case of AR 7978 during our computations (for higher values MDI saturates). The total magnetic flux reaches its maximum between the second and third solar rotation and returns to its pre-emergence level by the sixth rotation (for more details on the flux evolution, see Démoulin et al., 2002a; van Driel-Gesztelyi et al., 2003b).

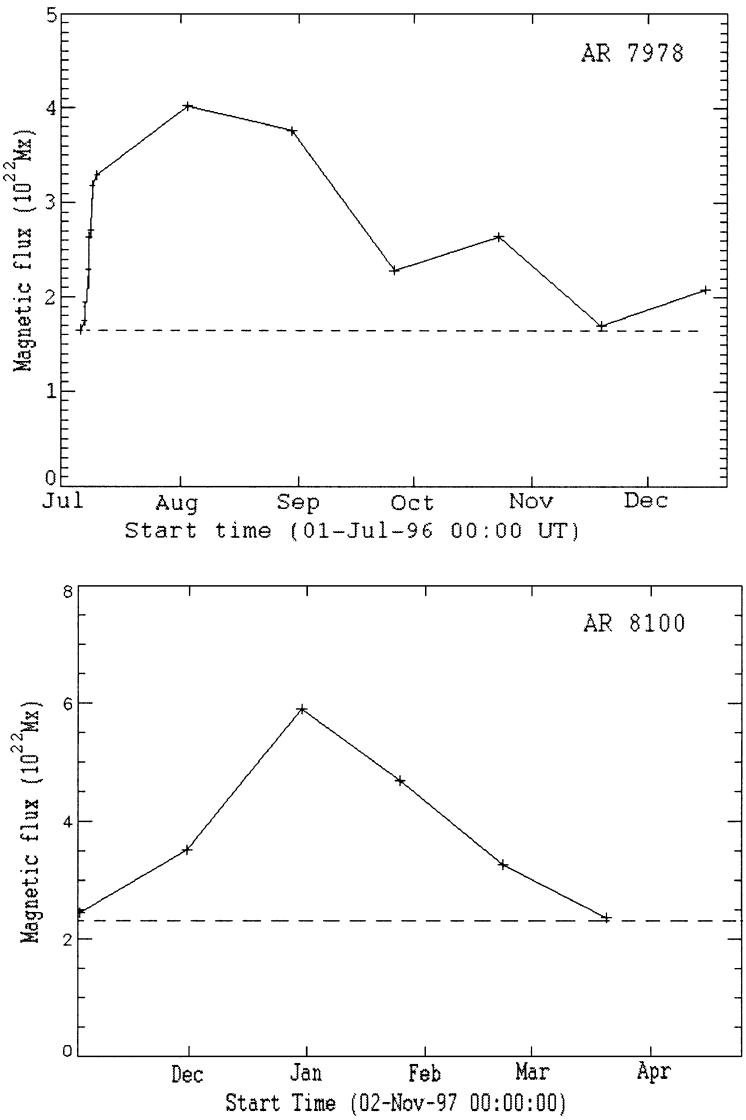

Figure 2. Evolution of the total magnetic flux (the sum of positive flux and absolute value of negative flux) versus time for AR 7978 (top panel) and AR 8100 (bottom panel). Longitudinal MDI magnetograms at each CMP have been used. The magnetic flux values have been corrected for underestimation in MDI measurements. The horizontal dashed line indicates the pre-emergence flux level.

All solar activity was dominated by AR 7978 during the last 6 months of 1996. During the emergence and the two following rotations, the AR produced numerous flares (including an X2.6 flare and CME event on July 9, see Dryer et al., 1998) until the disappearance of the main spots by September. On the other hand, CME activity, which was at first mainly related to flare events, continued at a high level for

TABLE I
Flare and CME activity in the ARs

	AR 7978				AR 8100			
Rot.	Date CMP	Flares	CMEs obs.	CMEs cor.	Date CMP	Flares	CMEs obs.	CMEs cor.
1	07 July 96	33	08	11	02 Nov. 97	35	16	24
2	02 Aug. 96	16	05	05	29 Nov. 97	07	–	02
3	30 Aug. 96	09	02	03	27 Dec. 97	16	06	12
4	25 Sept. 96	–	05	05	23 Jan. 98	06	09	17
5	23 Oct. 96	–	03	04	20 Feb. 98	–	04	10
6	19 Nov. 96	–	03	03	–	–	–	–
Total		58	26	31		64	35	65

The columns of the table give for each AR, respectively: the date of CMP corresponding to the rotation number shown in the first column, the number of flares for GOES X-ray classes from X to B, the number of observed CMEs and the corrected CME numbers (computed for each AR as explained in the text).

the next three rotations (van Driel-Gesztelyi et al., 1999). However, none of the late CMEs were related to flare events above the GOES B1 level. Table I lists the number of flares in all X-ray classes and of the observed CMEs. The flare data in Table I come from GOES X-ray and optical event catalog (http://www.lmsal.com/SXT/operations.html). CMEs have been analyzed using SoHO/Extreme Ultraviolet Imaging Telescope (EIT, Delaboudinière et al., 1995) and SoHO/Large Angle Spectroscopic Coronagraph (LASCO, Brueckner et al., 1995) observations. The low level of activity during the lifetime of AR 7978 allowed us to identify CMEs that could be originated in this AR even when it was on the far side of the Sun. The number of CMEs has been corrected because of data gaps assuming that the frequency of the CMEs is the same during these gaps as during observing times (Table I).

2.2. AR 8100 ALONG SIX SOLAR ROTATIONS

AR 8100 appeared on the solar surface on October 28, 1997, at S21 E67. This AR could be identified on the solar disk during six solar rotations, until March 1998. The AR emerged into a region of dominantly negative field and had a negative leading polarity, as is expected from the Hale–Nicholson law for solar cycle 23 (Hale and Nicholson, 1925). Several secondary bipoles emerged during the first solar rotation (compare top-left to top-right panel in Figure 3). Flux emergence continued as the AR rotated to the far side of the Sun. Magnetic flux increased until the third rotation when a new bipole emerged into the decaying AR close to CMP (Figure 2 bottom panel and Figure 3). The total magnetic flux values in the

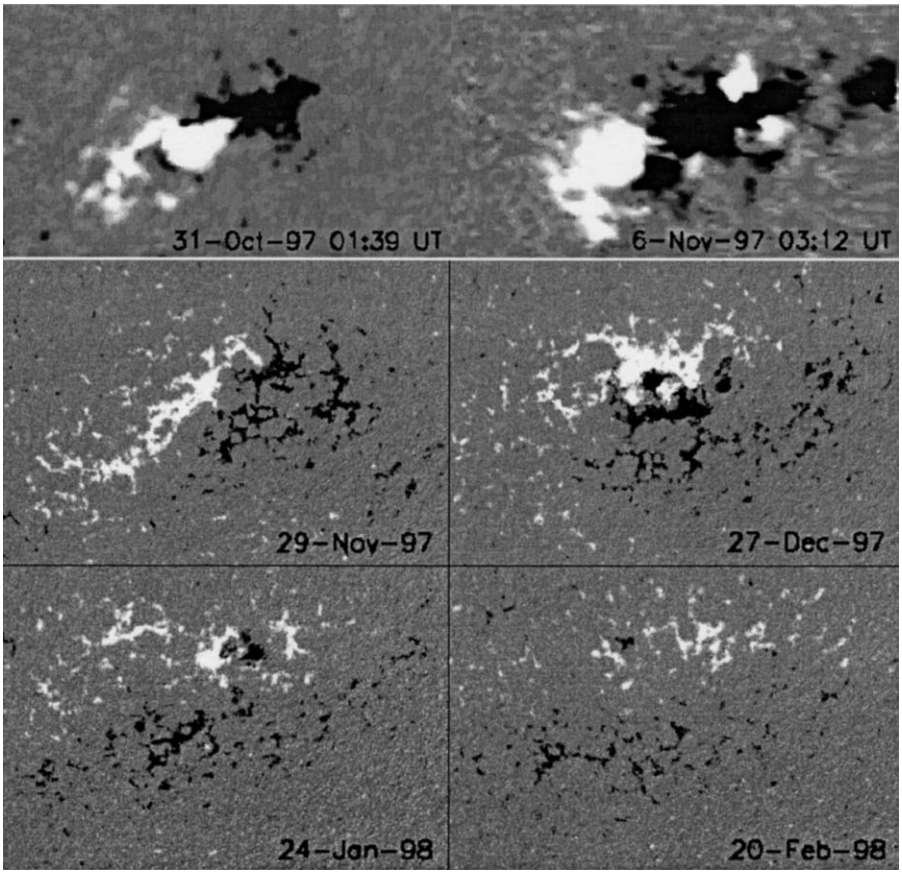

Figure 3. SoHO/MDI magnetic maps during five consecutive rotations of AR 8100. During the first transit of the AR (CMP on Nov. 2, 1997), several small bipoles emerged as shown in the two top panels. The sizes of these boxes are 310 × 178 Mm. The long-term evolution of AR 8100 from the second to the fifth rotation is shown in the central and bottom panels. The sizes of these boxes are 538 × 366 Mm (so they are larger to include the full AR compared to the top row). All the MDI maps have been obtained at or close to CMPs. The convention for the figure is the same as in Figure 1.

bottom panel of Figure 2 have been computed at each CMP over a constant area, and have been corrected for MDI underestimation (for a more detailed analysis of the magnetic flux evolution see Green et al., 2002).

Figure 3 shows the evolution of the AR along five solar rotations. The most remarkable feature in this figure is a clockwise rotation of the polarities through more than 150° from the initial configuration, in which the preceding spot is closer to the equator following Joy's law (Hale et al., 1919). Analyzing synoptic maps along 2.5 solar cycles, López Fuentes et al. (2003) found that ≈300 bipolar flux concentrations (≈15% of all bipoles) manifested significant rotation of the polarities around one another; this kind of motion has been interpreted as due to the emergence of deformed flux tubes. The evolution of the photospheric field of AR 8100 was

dominated by the rotation of the polarities, but flux emergence, magnetic field cancellation and differential rotation also played a role.

We will refer to the AR as 8100 over all the rotations, although in the second rotation it was identified as AR 8112, in the third as AR 8124, in the fourth as AR 8142, while no number was assigned in the fifth rotation.

AR 8100 was a highly flare and CME productive region during its first solar rotation (Green et al., 2001). Several flares and associated CMEs were observed, including an X9.4 class are on November 6, 1997 (Maia et al., 1999). Table I shows the number of flares observed by GOES (X-ray classes X to B), together with the observed and corrected CME numbers. The number of flares was determined as done for AR 7978. The number and importance of the flares decreased remarkably from the first to the second rotation, while during the third rotation they became high again. This increase could be caused by the emergence of new flux (Figure 3 central-right panel). Flare activity decreased by the fourth and disappeared by the fifth rotation. CME production was high throughout the AR evolution. Since AR 8100 was not alone on the solar disk, as was the case for AR 7978, the identification of CMEs starting from this AR is more difficult. LASCO and EIT data were combined with other low coronal signatures of CMEs, like filament disappearances in Hα or formation of cusps in Yohkoh/Soft X-ray Telescope (SXT, Tsuneta et al., 1991) (see Green et al., 2002 for details). The observed CME number was corrected for data gaps and far-side locations assuming that the CME frequency can be interpolated linearly between successive rotations. After all these corrections, we find that AR 8100 was the source of $\approx$65 CMEs.

3. The Magnetic Helicity Budget of the Analyzed ARs

3.1. General considerations

The magnetic helicity of a given field $\vec{B}$ within a volume V is defined as:

$$H = \int_V \vec{A} \cdot \vec{B}\, dV, \tag{1}$$

where the vector potential $\vec{A}$ satisfies $\vec{B} = \vec{\nabla} \times \vec{A}$. The computation of H is physically meaningful only when $\vec{B}$ is fully contained inside V (i.e. when the normal component of the field, $B_n = \vec{B} \cdot \hat{n}$, vanishes on the boundary S of V). However, Berger and Field (1984) have shown that for cases where $B_n \neq 0$ one can define a relative magnetic helicity (H_r) by subtracting the helicity of a reference field $\vec{B}_0$ (with $\vec{B}_0 = \vec{\nabla} \times \vec{A}_0$) having the same distribution of B_n on S:

$$H_r = \int_V \vec{A} \cdot \vec{B} \cdot dV - \int_V \vec{A}_0 \cdot \vec{B}_0\, dV. \tag{2}$$

Berger and Field (1984) and Finn and Antonsen (1985) have shown that H_r is gauge-invariant and does not depend on the common extension of $\vec{B}$ and $\vec{B}_0$ outside V. In this paper, we refer always to the relative magnetic helicity even when we do not use explicitly the subindex r.

As demonstrated by Berger (1984), H_r is a well preserved quantity under solar conditions. Then, the only way helicity can be modified inside a magnetic volume in the Sun is because of helicity flux crossing the boundary S. The relative helicity variation is given by Berger and Field (1984) as:

$$\frac{dH_r}{dt} = -2 \int_S [(\vec{A}_0 \cdot \vec{v})\vec{B} - (\vec{A}_0 \cdot \vec{B})\vec{v}] \ \vec{d}S, \tag{3}$$

where $\vec{v}$ is the velocity of the plasma. At the photospheric portion of S, the first term on the right-hand side of Eq. (3) represents the flux of helicity by plasma motions parallel to the photosphere (transverse component, v_t, of $\vec{v}$). These motions comprise braiding, twisting and shearing, which includes a well-known large-scale shearing motion, the surface differential rotation. The second term on the right-hand side of Eq. (3) corresponds to transport of helicity across S (with v_n, normal component of $\vec{v}$). At the photospheric portion of S, these motions include emergence (helicity inflow) and submergence of flux (helicity outflow); while at the upper high coronal portion of S ejection of CMEs is the main helicity outflow. When evaluating the magnetic helicity budget of an active region, we have to compute these two terms and compare them to the magnetic helicity contained in the coronal field. That is to say, we can write the magnetic helicity balance in an AR as:

$$\Delta H_{\text{cor}\cdot} = H_{\text{flux photos. motions}} - N \cdot H_{\text{CME}}, \tag{4}$$

where Δ denotes the variation of the coronal helicity ($H_{\text{cor.}}$), N is the number of ejected CMEs and H_{CME} is the mean helicity carried away per CME, computed as explained in Section 3.4. In $H_{\text{flux photos. motions}}$ we include: injection by large scale photospheric shearing motions (i.e. the differential rotation) and by localized motions, both parallel and orthogonal (emergence or submergence) to the photosphere. We estimate the helicity flux on the coronal portion of S by $N \cdot H_{\text{CME}}$ neglecting any possible transfer to surrounding coronal regions.

The quantitative study of the helicity flux by localized photospheric motions is a very recent research subject in Solar Physics. Several authors have computed the helicity injected in ARs by motions parallel to the photosphere (Chae, 2001; Chae et al., 2001; Kusano et al., 2002; Moon et al., 2002; Nindos and Zhang, 2002) using magnetic field observations and a local correlation tracking method to derive v_t. In general, the aforementioned papers have computed the magnetic helicity flux during a very short period of time as compared to the lifetime of an AR (being the longest $\approx$120 h, Kusano et al., 2002). The results of all these studies show that helicity injection by localized motions parallel to the photosphere is small when it

is compared to the helicity ejected by all the CMEs originated in an AR (see the review by van Driel-Gesztelyi et al., 2003a, and Section 3.4). The largest injection, 8.0×10^{42} Mx^2, was the one determined by Nindos and Zhang (2002) for AR 9165. However, it is possible that the local correlation tracking methods have serious intrinsic limitations (e.g., smoothing effects on the real velocities, non-detection of twisting motions), which combined with problems linked to the observations used (e.g., low spatial resolution of the magnetograms, lack of intensity contrast in high intensity field regions), results in a large underestimation of the amount of helicity injected by this kind of motions (see a detailed discussion in Démoulin and Berger, 2003).

In one of the studies mentioned above (Kusano et al., 2002), the authors also calculated the helicity flux across the photosphere. They derived v_t as discussed above and they computed v_n from the induction equation. Their results show that magnetic helicity was injected in AR 8100 by both kinds of motions, parallel and orthogonal to the photosphere, but these two helicity fluxes had opposite signs. Indeed, correlation tracking methods do not measure plasma motions, but rather the displacements of the photospheric cuts of magnetic flux tubes that are the result of both horizontal and vertical plasma motions. Démoulin and Berger (2003) have shown that when using the velocity deduced from a correlation tracking method, the full helicity flux (with the observational limitations mentioned above) is obtained, and thus adding both terms leads to incoherent results. The relatively small input of magnetic helicity is more inherent to the weaknesses of the tracking method than thought before.

For the two ARs analyzed in this paper, we have computed the variation of the coronal magnetic helicity along several solar rotations (Section 3.2), the photospheric inflow of helicity only by surface differential rotation (Section 3.3) and the outflow of helicity via CMEs (Section 3.4). These three values are confronted in Section 3.5, where we discuss our helicity budget and the relative importance of coronal helicity sources. We have not included the effect of flux submergence in the helicity budget because it should be small, as follows. During the long-term evolution, magnetic flux disappeared due to small scale cancellations and related submergence processes. However, because such reconnection processes occur low in the atmosphere, the main effect is to cut the original flux tube without bringing significant helicity below the photosphere. It mainly cuts the helicity channel of the involved field lines, the helicity flux from the convective zone is disappearing together with the photospheric magnetic flux.

3.2. Coronal magnetic helicity content

To compute $H_{\mathrm{cor.}}$, we have modelled the coronal field under the linear (or constant α) force-free field (lfff) assumption ($\vec{\nabla} \times \vec{B} = \alpha \vec{B}$) using a fast Fourier transform method, as proposed by Alissandrakis (1981). We have used SoHO/MDI

magnetograms close to CMPs of the studied ARs as boundary conditions of our extrapolations. The value of α is determined through an iterative process by comparing after each iteration the computed field lines to the soft X-ray loops observed with Yohkoh/SXT (see Démoulin et al., 2002a; Green et al., 2002 for details). Figures 4 and 5 illustrate the evolution of the coronal shear for AR 7978 and AR 8100, respectively.

Following the results by Berger (1985), the relative coronal magnetic helicity can be written as:

$$H_{\text{cor.}} = 2\alpha \sum_{n_x=1}^{N_x} \sum_{n_y=1}^{N_y} \frac{\left|\tilde{B}^2_{n_x,n_y}\right|}{l\left(k_x^2 + k_y^2\right)}, \tag{5}$$

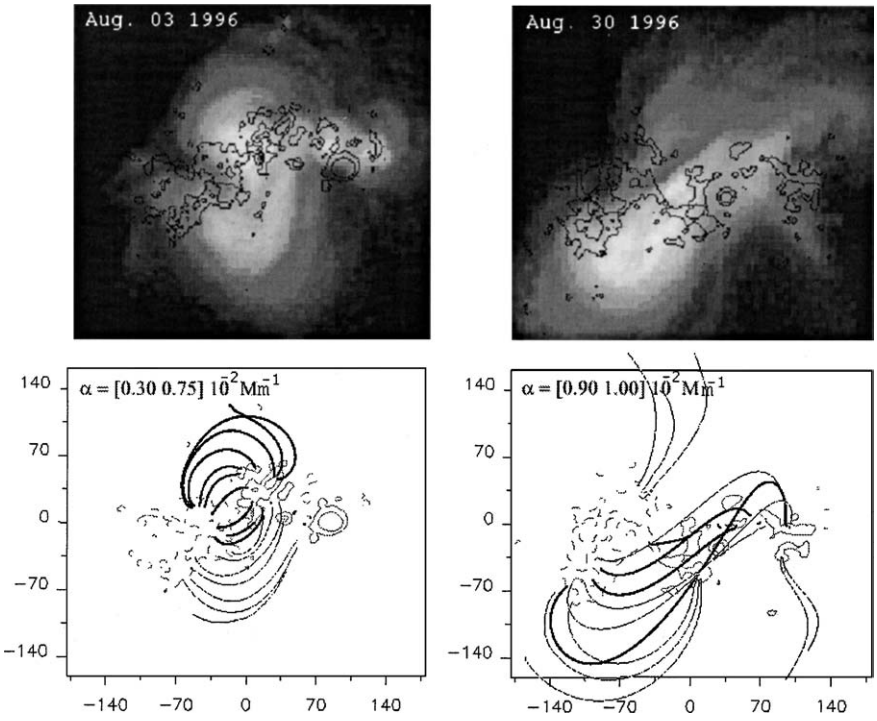

Figure 4. Yohkoh/SXT observations and linear force-free computations of the coronal field of AR 7978 from the second to the fifth rotation. The α value is selected to have the best global match between the SXT loops and the computed field lines. For this particular AR the magnetic field presents a North–South shear gradient. We have represented in the same figure with thick (thin) continuous lines the field lines computed taking the highest (lowest) value of α, these two values are shown as an interval in the top-left corner of the corresponding figures. The abscissas and ordinates in each map are expressed in Mm. Isocontours ($\pm$100, 500, 1000 G) of the line of sight magnetic field have been drawn with continuous/dashed lines for positive/negative values.

(*Continued on next page*.)

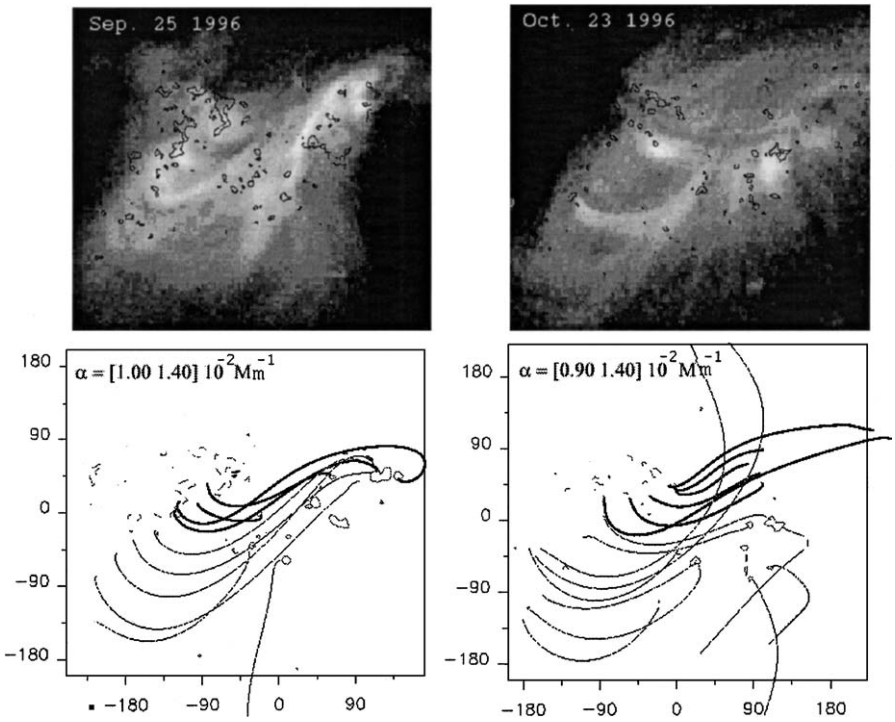

Figure 4. (*Continued*).

where x, y are the cartesian horizontal coordinates, $\tilde{B}_{n_x,n_y}$ is the Fourier amplitude of the harmonic (n_x, n_y), $l = \sqrt{k_x^2 + k_y^2 - \alpha^2}$, $k_x = 2\pi n_x/L$, $k_y = 2\pi n_y/L$, being L the horizontal extension of the computational box. As L is at the denominator, this expression becomes infinite at each resonant value of α: $\alpha_r = \sqrt{k_x^2 + k_y^2}$. A way to avoid high artificial helicity values close to the resonance values is to use a linearized version of Eq. (5) versus α (Green et al., 2002):

$$H_{\text{lin}} = 2\alpha \sum_{n_x=1}^{N_x} \sum_{n_y=1}^{N_y} \left|\tilde{B}^2_{n_x,n_y}\right| \left(k_x^2 + k_y^2\right)^{-3/2}. \tag{6}$$

This expression, which gives a lower bound for the magnetic helicity deduced from a lfff extrapolation, is used for the values in the second columns of Tables II and III. We want to stress that we have used the same size of the integration box for all the extrapolated magnetograms of each CMP, and that α stayed below its resonant value in all cases. The values of $H_{\text{cor.}}$ suffer from the limitations of lfff models that are approximate representations of the real field. The general property of a lfff is to shear the shorter field lines less, and the longer field lines more, than the observed

coronal loops. This implies that the magnetic helicity will be underestimated in the smaller scales, and overestimated in the larger ones, compared to its true value. However, the order of magnitude of the obtained values agrees quite well with theoretical expectations, and thus our results are expected to be reasonably good estimates (see Tables II and III). In the following paragraphs we discuss particular aspects of each AR.

In AR 7978, not all SXT loops observed at a given time can be represented using the same value of α. In general, a shear gradient exists in the North-South direction (see a detailed analysis in Mandrini et al., 2000, 2001). Figure 4 illustrates the temporal evolution of the coronal shear from the second to the fifth rotation. The maximum and minimum values of α shown in each figure correspond to the North and South portion of the AR, respectively. The value of α stays always positive as expected for a southern-hemisphere AR following the hemispheric chirality-rule, positive helicity is dominant in this hemisphere (see van Driel-Gesztelyi et al.,

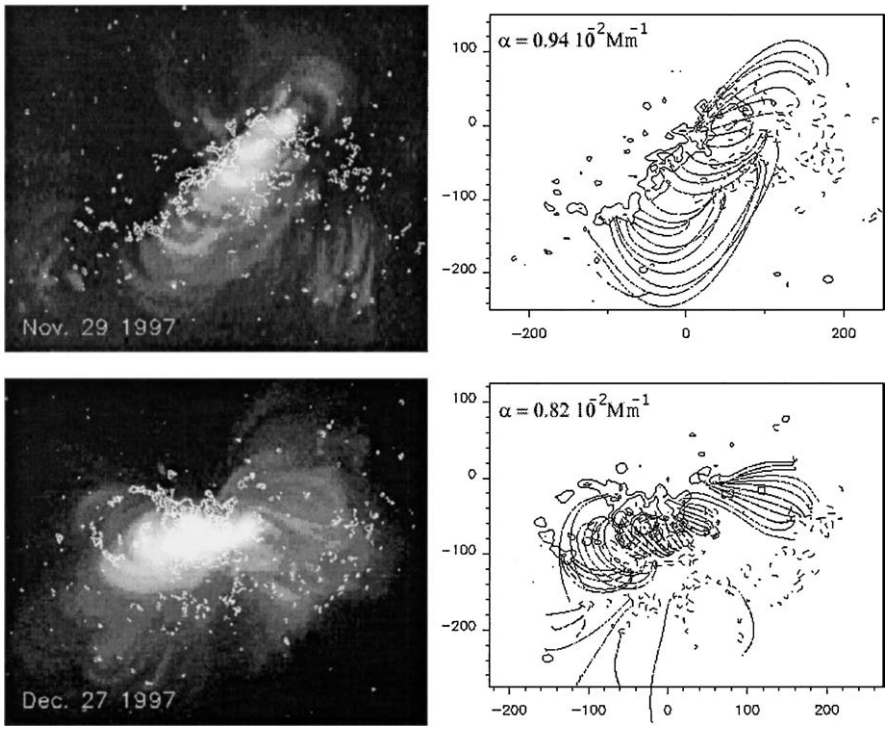

Figure 5. Yohkoh/SXT observations and linear force-free computations of the coronal field of AR 8100 from the second to the fifth rotation. The α value used for each model is shown on the top-left corner of the corresponding figure. The abscissas and ordinates in each map are expressed in Mm. Isocontours ($\pm$50, 200, 500 G) of the line of sight magnetic field have been drawn with continuous/dashed lines for positive/negative values.

(*Continued on next page*.)

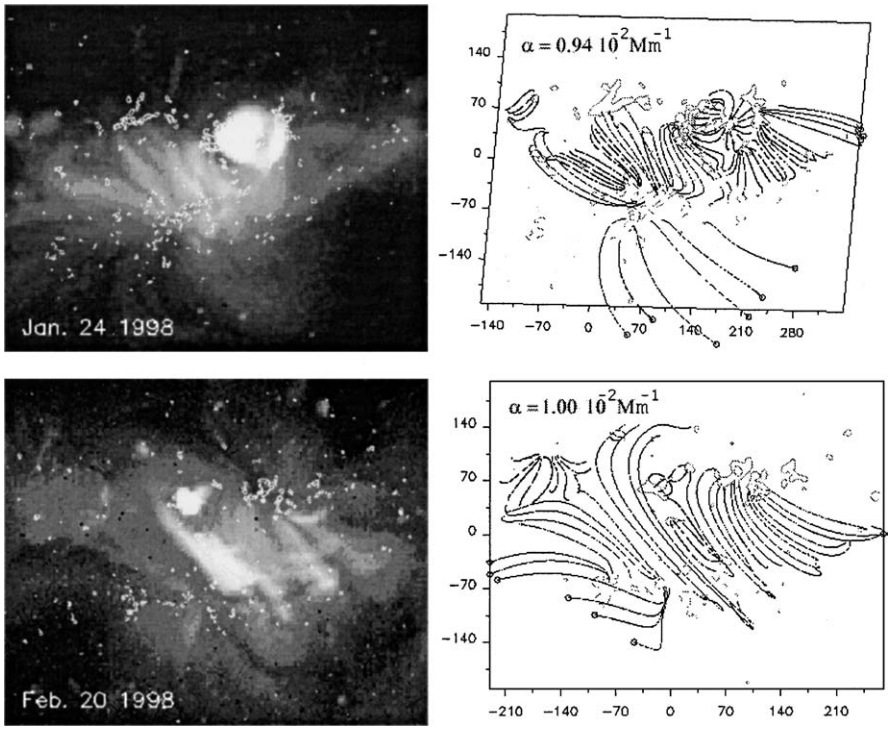

Figure 5. (*Continued*).

2003a, and references therein). For AR 7978, the coronal magnetic helicity (see Table II) has been computed within the interval given by the values of α. We estimate that the error in the determination of the best α value is $\approx$25% and thus this is also the error in the computed linearized helicities. Because of the proximity of the decaying AR, which had a helicity sign opposite to that of AR 7978 (see Mandrini et al., 2000), $H_{\mathrm{cor.}}$ cannot be computed for AR 7978 alone during the first rotation. This rotation is then excluded from the totals shown in the last line in Table II. The value between parenthesis for the sixth rotation (Nov. 18) is only indicative. It was obtained for the coronal model of the southern portion of AR 7978, the SXT loops in the North were so faint that it was not possible to model them.

In AR 8100 α takes a negative value during the first rotation (Green et al., 2002), this means that this AR does not follow the hemispheric chirality-rule. From the second rotation on, the value of α stays positive and almost constant (see Figure 5). Computing the value of α from Nov. 2 to 5, we have found that it changes from -1.3×10^{-2} Mm^{-1} to -0.63×10^{-2} Mm^{-1}, becoming less negative. We interpret this change as being due to the emergence of a new bipole in AR 8100 which presumably carries positive helicity, that is to say of opposite sign to the primary one.

TABLE II
The magnetic helicity budget of AR 7978 (listed per rotation)

Date Rot.	$\Delta H_{\text{cor.}}$	$\langle \Delta H_{\text{cor.}} \rangle$	$H_{\text{d.r.}}$	$\langle \Delta H_{\text{cor.}} \rangle - H_{\text{d.r.}}$	$\Delta H_{\text{m.cl.}}$ (CME obs.)	$\Delta H_{\text{m.cl.}}$ (CME cor.)
July 07						
1			0.4		[16.,64.]	[22.,88.]
Aug. 03	[10.,22.]					
2		24.	6.0	18.	[10.,40.]	[10.,40.]
Aug. 30	[34.,46,]					
3		−19.	6.0	−25.	[4.,16.]	[6.,24.]
Sept. 25	[18.,24.]					
4		−11.	2.0	−13.	[10.,40.]	[10.,40.]
Oct. 23	[8.,12.]					
5		(−2.)	1.6	−3.6	[6.,24.]	[8.,32.]
Nov. 19	(8.)					
6		(−3.)	0.6	−3.6	[6.,24.]	[6.,24.]
Total 2–6		−11.	16.2	−27.2	[36.,144.]	[40.,160.]

An interval of helicity ($\Delta H_{\text{cor.}}$) is given for the corona because of the observed shear gradient. These values and their variations ($\langle \Delta H_{\text{cor.}} \rangle$, the difference between averages of consecutive rotations) are computed from the successive CMP magnetograms. Corrections have been done for MDI underestimated measurements to $H_{\text{cor.}}$, $\Delta H_{\text{cor.}}$ and $\Delta H_{\text{d.r.}}$. The helicity in the MCs ($\Delta H_{\text{m.cl.}}$) is given taking the two limits for their length (0.5 and 2 AU) for both the observed and corrected CME numbers. All values are in units of 10^{42} Mx^2.

3.3. Magnetic helicity injected by photospheric shearing motions

For the computation of the magnetic helicity injected by photospheric plasma motions parallel to the surface, Berger (1984, 1988) derived an expression for the first term in Eq. (3) that depends only on observable photospheric quantities. Berger (1986) first showed that this helicity flux could be understood as the summation of the rotation rate of all the individual elementary flux pairs weighted by their magnetic flux; then, the helicity injection rate by these horizontal motions writes

$$\frac{dH_r}{dt} = -\frac{1}{\pi} \int_S \int_S \frac{R \times \vec{v}(\vec{r})}{R^2} B_n(\vec{r}) B_n(\vec{r'})\, dS\, dS', \tag{7}$$

where $\vec{R} = \vec{r} - \vec{r'}$ is the difference in spatial positions on the photospheric plane. This equation involves a double integration on the photospheric boundary. Using this result, Démoulin et al. (2002b) analyzed helicity injection in synthetic bipolar

TABLE III
Idem Table II for AR 8100

Date Rot.	$H_{\mathrm{cor.}}$	$\Delta H_{\mathrm{cor.}}$	$\Delta H_{\mathrm{d.r.}}$	$\Delta H_{\mathrm{cor.}} - \langle \Delta H_{\mathrm{d.r.}} \rangle$	$\Delta H_{\mathrm{m.cl.}}$ (CME obs.)	$\Delta H_{\mathrm{m.cl.}}$ (CME cor.)
Nov. 2–5	–	−67.2	[0.4,1.6]	−66.2	[−20.,−80.]	[−20.,−80.]
Nov. 02	−22.0					
1		67.0	[2.8,10.2]	60.4	–	–
Nov. 29	45.0					
2		−5.8	[10.2,−9.2]	−6.4	[0.,0.]	[5.,20.]
Dec. 27	39.2					
3		−22.4	[−9.2,−5.6]	−15.0	[12.,48.]	[24.,96.]
Jan. 23	16.8					
4		−6.6	[−5.6,−3.2]	−2.2	[18.,72.]	[34.,136.]
Feb. 20	10.2					
5		−4.0	−3.2	−0.8	[8.,32.]	[19.,76.]
Total 2–5		−38.8	−14.6	−24.4	[38.,152.]	[82.,328.]

The total budget on the last line is the sum from the second to the fifth rotation. We have analyzed separately the budget from Nov. 2 to 5 because of the change in α during the first rotation. Furthermore, a range is given for the helicity injected by the differential rotation ($\Delta H_{\mathrm{d.r.}}$) (see text). Values for the ejected helicity are shown as in Table II. Corrections have been done for MDI underestimated measurements to $H_{\mathrm{cor.}}$, $\Delta H_{\mathrm{cor.}}$ and $\Delta H_{\mathrm{d.r.}}$ as in Table II. All values are in units of 10^{42} Mx^2.

configurations. We consider different velocity profiles for localized shearing motions and large scale differential rotation. We have shown that injection by horizontal photospheric plasma motions could be separated in two different helicity terms: the rotation of each polarity on itself injects *twist* helicity, while the rotation of each polarity relative to the opposite polarity generates *writhe* helicity. Then, helicity injection could be written as

$$\begin{aligned} \Delta H_r(t) &= -\frac{1}{2\pi} \int\int_{B_n \cdot B_n' > 0} \Delta\theta \, B_n B_n' \, dS \, dS' \\ &\quad + \frac{1}{2\pi} \int\int_{B_n \cdot B_n' < 0} \Delta\theta \, |B_n B_n'| \, dS \, dS' \\ &= \Delta H_r(t)|_{\mathrm{twist}} + \Delta H_r(t)|_{\mathrm{writhe}}, \end{aligned} \tag{8}$$

where Δ refers to a variation between two different times and $\Delta\theta = (\vec{R} \times \Delta\vec{R})/R^2|_n$.

Within horizontal photospheric motions, the main candidate to inject magnetic helicity in the corona is the differential rotation because its velocity profile is

both spatially and temporally coherent. However, DeVore (2000) computed the helicity injected by this motion on synthetic flux concentrations and found that it does not provide a monotonous helicity inflow (see Figures 1 and 2 of DeVore, 2000). The results of DeVore (2000) were extended by Démoulin et al. (2002b), who analyzed the role of twist and writhe helicities in the injection. We have found that twist and writhe helicity fluxes have always opposite signs and, as their magnitudes are similar, they partially cancel. The relative importance of twist and writhe helicity injection by differential rotation depends mainly on the orientation of the bipole. Twist helicity dominates when the bipole is parallel to the equator, while writhe dominates when it is perpendicular. The two terms, because of their similar magnitudes, cancel when the angle (the active region tilt) formed between the bipole axis and the solar equator is 45°. This means that if the orientation of an AR is changing with time, the helicity injection rate by the differential rotation will also change. This explains the non-monotonous evolution of the helicity flux found by DeVore (2000). We found that in all cases that could be reasonably applied to observed shearing motions the maximum helicity injected was $\leq 0.3\ \Phi^2$, being Φ the average flux of both polarities.

In the following paragraphs we will compute the helicity injection by differential rotation in AR 7978 and AR 8100. The results (see Tables II and III) have been obtained taking as initial conditions the MDI magnetograms at CMPs (Figures 1 and 3). These initial configurations are evolved applying differential rotation along one Carrington rotation, and the integrated helicity is computed. We want to stress that the values for the helicity injection by differential rotation in Tables II and III are perhaps the most reliable ones in all our helicity budget analysis.

The magnetic helicity injected in AR 7978 per solar rotation is summarized in the fourth column of Table II. Except during the strong flux emergence period (July 4–10, 1997) in the first rotation, localized horizontal motions were no evident in this AR; the second flux emergence episode started when the AR was on the invisible side of the Sun. As mentioned in Section 2, the long-term evolution of the photospheric field was mainly dominated by the differential rotation and magnetic diffusion (see Figure 1). As shown in Démoulin et al. (2002b), the generation rate of helicity is larger when the bipole tilt is small (values for the second and third rotations). This injection declines as the bipole gets closer to 45° (fourth and sixth rotations). The total helicity injected in AR 7978 by the differential rotation is $\approx 1.6\ 10^{43}\ \mathrm{Mx}^2$.

The trend of the helicity injection rate in AR 8100 is quite different from that of AR 7978 (see the fourth column in Table III). As discussed in Section 2, it is probable that the sign of the coronal magnetic helicity had changed around the end of the first rotation due to new flux emergence carrying positive helicity, thus we have computed separately the helicity injection from Nov. 2 to 5 (first line in Table III). The helicity injection is given as a range because flux emergence during the first three rotations (Figures 3 and 2 bottom panel) changes the distribution

of the photospheric field, then the true value should be different from the one obtained when only distributions at CMPs are considered. The helicity injection rate by differential rotation changes sign as AR 8100 evolves and rotates (see Figure 6 top panel). This is due to the change in the AR tilt angle (Démoulin et al., 2002b). Initially, AR 8100 is more oriented in the East–West direction and positive helicity is injected (twist helicity dominates). After, it becomes more oriented in the North–South direction and negative helicity is injected (writhe helicity dominates). The magnetic polarities in AR 8100 are rotating not only due to the effect of the differential rotation, but also because of a large intrinsic rotation as seen in Figure 3 and illustrated in the polar plot of Figure 6 (bottom panel). López Fuentes et al. (2003) have interpreted this behavior as due to the emergence of a flux tube deformed by external motions. Considering the full period, from the second to the fifth rotation, the total helicity injected into AR 8100 by differential rotation is $\approx -1.5 \times 10^{43}$ Mx^2.

Strong shearing motions were evident in magnetogram movies during the first rotation of AR 8100. Kusano et al. (2002) analyzed helicity injection by this kind of motions from Nov. 2 to 6 using a local correlation tracking method. They found that the net helicity inflow was negative ($\approx -4 \times 10^{42}$ Mx^2), with most of it injected between Nov. 3 and 5. However, they also observed that helicity injection was positive in some AR locations, but a negative injection, much stronger in magnitude, was present in the high intensity field regions (see Figures 4c and 6c from Kusano et al., 2002). This represents the dominant flux of helicity and produces the dominant negative helicity in the corona during these days. Moon et al. (2002) also investigated the contribution of localized shearing motions on a much shorter time period (6.5 h, from 21:38 UT on Nov. 3 to 4:00 UT on Nov. 4). They used a local correlation tracking method as done by Chae (2001), which is different from that of Kusano et al. (2002). Still, the results of Moon et al. are fully consistent with those of Kusano et al. Their mean injection rate (-1.7×10^{42} Mx^2) and spatial distribution of the helicity are comparable during the interval of time studied by Moon et al. (2002) (compare Figure 5a in Moon et al. (2002) to Figure 6c in Kusano et al. (2002)).

3.4. Magnetic helicity ejected via CME

Interplanetary magnetic flux tubes are the trace of plasmoids ejected from the Sun. Magnetic clouds (MCs), a subset of interplanetary flux tubes, are characterized by a coherent rotation of their magnetic field. *In situ* measurements of the three components of their field can be well described by a linear force-free model in cylindrical geometry (see e.g., Lepping et al., 1990, 1997; Marubashi, 1997; Shimazu and Marubashi, 2000). Since we have no way to compute the helicity in a CME, we have assumed a one to one correspondence with MCs (see e.g. Webb et al., 2000). Following Berger (1999), we have derived a numerical expression for the magnetic

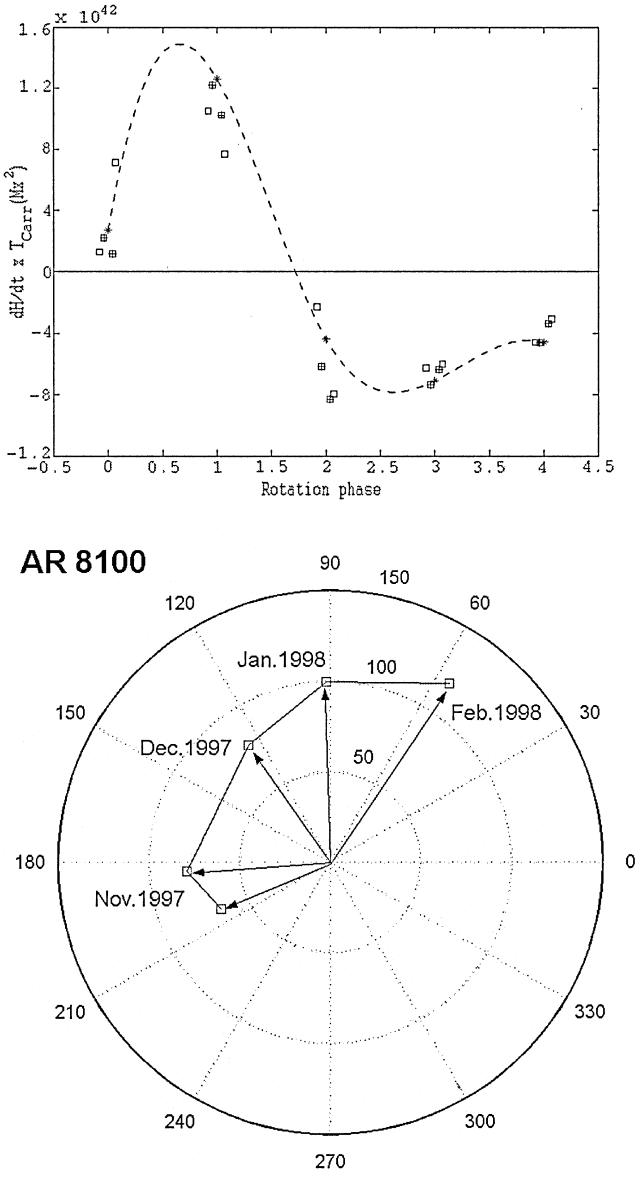

Figure 6. The magnetic helicity injection by differential rotation in AR 8100. In the top panel, the evolution of the injection rate ($dH_r/dt \cdot T_{\mathrm{Carr}}$) by differential rotation vs. time is shown (T_{Carr} is the Carrington rotation period). Rotation phase 0 corresponds to Nov. 2, 1997. MDI magnetograms at each CMP (asterisks), ± 1 (squares with a cross) and ± 2 days (squares) from CMP have been used to compute dH_r/dt. A spline curve computed using only the CMP values has been added. In the bottom panel we illustrate the rotation of the polarities in AR 8100 by means of a polar plot. This rotation is the main origin of the change in sign of helicity injection shown in the top panel. The center of the polar plot corresponds to the position of the center of the negative polarity at CMPs, while the arrows point to the relative position of the positive polarity. The tilt angles are shown as measured on the Sun.

helicity in a twisted interplanetary flux tube (Démoulin et al., 2002a):

$$\frac{dH_{\text{m.cl.}}}{dz} \approx 0.70 B_o^2 R^3, \tag{9}$$

where B_0 is the tube axial magnetic field and R its radius. We have evaluated the mean magnetic helicity in a MC using average values of $B_0 = (2.0 \pm 0.7) \times 10^{-4}$ G and $R = (2.1 \pm 0.7) \times 10^{12}$ cm for a set of 18 clouds studied by Lepping et al. (1990). The same computation has been done for another sample of 23 clouds analyzed by Zhao et al. (2001) with $B_0 = (2.4 \pm 0.8) \times 10^{-4}$ G and $R = (1.7 \pm 0.8) \times 10^{12}$. All these cloud values are derived from *in situ* measurements at 1 AU from the Sun. For the length of the interplanetary flux tube we have considered two different values: $L_1 = 0.5$ AU as done by DeVore (2000) and $L_2 = 2.0$ AU, which gives four times as much helicity for one average CME. In this last case we are assuming that the cloud is still anchored to the Sun (e.g. Richardson, 1997). Figure 7 shows the distribution of the relative magnetic helicity in the two previous samples. What is striking is the widespread in the values of $H_{\text{m.cl.}}$. This means that the helicity ejected in a CME, which we will take as 2.0×10^{42} Mx^2 for a length of 0.5 AU, is perhaps the most uncertain value in our budget. Furthermore, we do not know how the twist is distributed along the MC, and a reasonable assumption we can make is that it is uniform.

The helicity ejected by each AR is computed multiplying the number of CMEs (observed and corrected) by the mean helicity in a cloud (see Tables II and III). AR 7978 is the source region of 31 corrected (26 observed) CMEs, while AR 8100 produced 65 corrected (35 observed) CMEs. These numbers are much higher than previously inferred (≈4–5 CMEs per AR along its lifetime), based on Solar Maximum Mission (SMM) observations (see e.g. DeVore, 2000). This implies that, in fact, a huge amount of helicity can be ejected from ARs along their lifetime (see last line in Tables II and III).

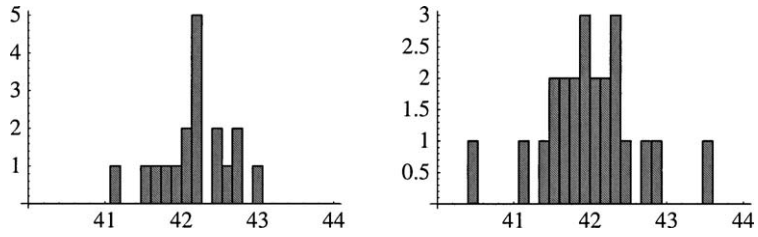

Figure 7. Distribution of the relative magnetic helicity of magnetic clouds (MCs) computed from the axial magnetic field intensity and radius measured in two samples by Lepping et al. (1990) (18 MCs, left panel) and Zhao et al. (2001) (23 MCs, right panel). The two samples overlap, since 11 clouds are the same in both studies, though they use different fitting models (in the newer sample the expansion of the flux tube during spacecraft crossing is taken into account). The mean relative magnetic helicity values are 2.4×10^{42} Mx^2 and 2.8×10^{42} Mx^2, respectively, assuming a 0.5 AU flux tube length.

3.5. COMPARING THE TERMS IN THE HELICITY BUDGET

Comparing the terms in the magnetic helicity balance equation (Eq. (4)), we now attempt to determine which is the main source providing helicity to the corona.

We have only computed the magnetic helicity inflow due to the differential rotation for the term including injection by photospheric motions. DeVore (2000) has also calculated this injection in a synthetic magnetic configuration and concluded that differential rotation was providing enough helicity to account for all the CMEs ejected during the lifetime of an AR. However, his study was based in early SMM observations. These data indicated that the number of CMEs associated with an AR was much lower than presently known. When we compare the values in the fourth columns of Tables II and III to those in the sixth and seventh columns, we find that the injection of magnetic helicity by differential rotation is negligible to account for the observed CMEs even for the smaller length of the interplanetary flux tube ($L1 = 0.5$ AU), which is reasonable to consider. The only exception is the second rotation of AR 8100. We conclude that, in general, the photospheric differential rotation cannot provide enough helicity to the CMEs. Nindos and Zhang (2002) reached the same conclusion from the analysis of a particular event where they identified the magnetic cloud associated to the solar CME.

The differential rotation is also a very inefficient helicity generator when we compare its injection to the change in the coronal helicity of both ARs (columns four and three in Tables II and III). In AR 7978, the differential rotation was injecting helicity of the same sign throughout the studied six solar rotations, but this amount stayed (except during the fifth rotation) one order of magnitude lower than the coronal change. During all this period CMEs were depleting the corona from magnetic helicity in a much larger amount than the coronal change.

The evolution of AR 8100 presents two different periods, one during which the AR helicity was negative (Nov. 2 to 5, 1997) and a second one when it was positive (from the second to the fifth rotation, we exclude the first rotation because of the uncertainty in the sign of the ejected helicity). Table III shows (Nov. 2–5 values) that the differential rotation cannot provide enough helicity to change the coronal helicity sign (compare the third to the fourth column) by two orders of magnitude. Furthermore, differential rotation injected helicity opposite in sign to the coronal one. During the second rotation the helicity injection by differential rotation became negative in sign, then it can deplete helicity from the corona. The helicity depletion by differential rotation agrees with the helicity variation in the corona in the last two rotations, and is smaller before.

The other two candidates that can provide helicity to the corona are localized horizontal photospheric motions and flux emergence (motions orthogonal to the photosphere). The fifth columns of Tables II and III give the difference between the change in the coronal helicity and the one injected by differential rotation. Adding numbers in this column to the ones of the last two columns (considering

either observed or corrected CME numbers), we have an estimate of the helicity photospheric motions, other than differential rotation, should provide. We will call this summations as $\Delta H_{\text{emerg.}}$.

Relative motions of the polarities were evident in AR 7978 during the two main flux emergence phases. After this period, there was no indication of significant shearing motions except the differential rotation. Helicity injection by horizontal motions was not computed for this AR. In AR 8100 shearing motions have been studied in detail by using local correlation tracking methods by Moon et al. (2002) (6.5 h from Nov. 3 to 4) and Kusano et al. (2002) (120 h from Nov. 2 to 6) (see Section 3.3). The amount of injected helicity obtained in these works ($\approx -4 \times 10^{42}$ Mx^2 or, in fact, -8×10^{42} Mx^2 if we correct this value by MDI underestimated measurements) can explain only 12% of the coronal helicity change ($\approx -67 \times 10^{42}$ Mx^2), and from 10 to 40% of the estimated helicity ejected in CMEs. As shown by Démoulin and Berger (2003) both flux emergence and shearing motions are included in the velocity that is determined by local correlation tracking methods (see Section 3.1); therefore, they include both helicity fluxes. However, these methods have serious limitations that may result in large underestimations of the injected helicity. So, further studies are needed to improve the estimates of the photospheric helicity fluxes (see the discussion about the study of helicity emergence by Kusano et al., 2002, in Section 3.1).

Does a buoyant twisted flux tube bring to the corona the helicity ejected in CMEs? The helicity of a twisted flux rope with a uniform twist across its section and having N number of turns is simply N, if it is measured in units of its flux to the second power. For AR 7978, 62–248 $\times 10^{42}$ Mx^2 of magnetic helicity should be provided to the corona to account for all the CMEs, including those in the first rotation (corrected numbers, last column in Table II). If we express these values in units of the square of the magnetic flux of the AR (that we estimate to be in average $\Phi \approx 1.5 \times 10^{22}$ Mx), we obtain 0.3–1.1 Φ^2. This shows that 31 CMEs carried away the equivalent helicity contained in the flux tube forming the AR having around one turn. If we do the same estimation for AR 8100, using the corrected CME numbers from the second to the fifth rotation (excluding the first rotation for uncertainties in the helicity sign ejected by CMEs) and an average flux $\Phi \approx 2.0 \times 10^{22}$ Mx, we obtain 0.2–0.8 Φ^2 meaning that 41 CMEs carried away the total helicity in the flux tube that formed this AR having less than one turn. The results are the same if we instead use ΔH_{emerg}. for the budget of both ARs. Moreno-Insertis and Emonet (1996) and Emonet and Moreno-Insertis (1998) showed that flux tubes need to be twisted by a few turns to be able to survive their rise through the convection zone. Though recent simulations by Abbett et al. (2001) indicated that the Coriolis force may also have a stabilizing effect on rising flux tubes, the need for them to be twisted did not disappear. Thus, the twist obtained from the helicity budgets seems to lie in the right range. Therefore, we may say that most of the helicity ejected in CMEs is generated below the photosphere and emerges with the magnetic flux.

4. Conclusions

We have studied in detail the long-term evolution of two ARs, AR 7978 and AR 8100, that were observed on the solar disk for six and seven solar rotations (Démoulin et al., 2002a; Green et al., 2002). AR 7978 was the only large AR on the solar disk from July 1996 to January 1997. AR 8100 was observed from November 1997 to March 1998. These regions were the source of numerous flares and CMEs along their lifetime, 31 and 65 CMEs, respectively, when CME observations are corrected because of data gaps and far side locations.

Flare activity started at a high level in the two ARs accompanied by CMEs. As the ARs evolved into their decay phase, the number as well as the importance of flares decreased, but still the CME activity stayed high. This evolution is most notable in AR 7978 where flares disappear by the third rotation. Though masked during the third rotation, because of flux emergence, the same behavior is observed in AR 8100. This indicates that, even if flares and CMEs share some common physics (like the instability of the magnetic field and magnetic reconnection), they are distinct phenomena. The flare importance and the number of flares depend more on the free magnetic energy which is available locally (e.g., formation of strong current layers), while the CME production seems to depend more on global quantities, in particular the amount of magnetic helicity.

In this study we put emphasis in the determination of the magnetic helicity balance of the ARs, and try to evaluate the relative importance of the sources providing helicity to the coronal field. As magnetic helicity remains invariant under solar conditions, even in resistive MHD, this quantity can be used as a trace to understand the evolution of the magnetic field from sub-photospheric layers to the corona and its ejection into the interplanetary medium. To draw the magnetic helicity balance of both ARs we have computed the variation of the coronal helicity, the injection by surface differential rotation and the ejection via CMEs.

Leaving aside particular aspects of the evolution of each AR that are reflected in their helicity budget, we have found for both of them that the photospheric differential rotation is a very ineffective generator of coronal magnetic helicity. This time-independent large-scale shear flow cannot provide either the required magnetic helicity to the coronal field (staying, in general, one order of magnitude lower, and, in some cases, injecting helicity of opposite sign to the coronal one) or to the field ejected into the interplanetary space. CMEs carry away at least 10 times more helicity than the one provided by differential rotation.

Considering the results from theoretical models of flux tube emergence, we have found that the helicity ejected via all the CMEs in these ARs can be provided by the end-to-end helicity of the flux tubes forming them. Thus, the dominant source of the coronal and interplanetary helicity is the inherent twist of these tubes. Magnetic helicity should be transferred from the sub-photospheric layers to the corona if we want to explain the existence of CMEs in all solar rotations. There is clear evidence

of flux emergence during the first and second rotation of AR 7978, and until the third rotation of AR 8100, that can account for the required helicity. However, we have no evidence of emergence during later rotations of the ARs. This long-term input of magnetic helicity can be simply provided by the magnetic flux tube if it continues to move across the photosphere, requiring that it stays buoyant (see López Fuentes et al. (2000) for evidence of this). An alternative mechanism to this extended emergence has been considered by Longcope and Welsch (2000). They propose that for the steady state the coronal helicity is determined by the amount of twist present in the sub-photospheric part of the flux tube, and that magnetic helicity transfer is provided by torsional Alfvén waves.

Acknowledgements

C.H.M. and P.D. acknowledge financial support from ECOS (France) and SECyT (Argentina) through their cooperative science program (A01U04). L.v.D.G. is supported by the Hungarian Government grants OTKA T-032846 and T-038013, and by Research Fellowship F/02/035 of the K.U. Leuven. We are grateful to the Royal Society for the award of a European Joint Project grant. L.M.G. thanks PPARC for postdoctoral funding. M.C.L.F. is supported by NASA and ONR. The authors thank the MDI, EIT and LASCO consortia and the Yohkoh/SXT team for their data. SoHO is a project of international co-operation between ESA and NASA. Yohkoh is a mission of the Japanese Institute for Space and Astronautical Science. We acknowledge the SURF for providing data for this publication.

References

Abbett, W.P., Fisher, G.F. and Fan, Y.: 2001, *Astrophys. J.* **546**, 1194.
Alissandrakis, C.E.: 1981, *Astron. Astrophys.* **100**, 197.
Berger, M.A.: 1984, *Geophys. Astrophys. Fluid. Dynamics* **30**, 79.
Berger, M.A.: 1985, *Astrophys. J. Sup.* **59**, 433.
Berger, M.A.: 1986, *Geophys. Astrophys. Fluid. Dynamics* **34**, 265.
Berger, M.A.: 1988, *Astron. Astrophys.* **201**, 355.
Berger, M.A.: 1999, *Geophys. Mon.* **111**, 1.
Berger, M.A. and Field, G.B.: 1984, *J. Fluid. Mech.* **147**, 133.
Berger, T.A. and Lites, B.W.: 2003, *Solar Phys*. **213**, 213.
Bothmer, V. and Schwenn, R.: 1994, *Space Sci. Rev.* **70**, 215.
Brueckner, G.E., Howard, R.A., Koomen, M.J., Korendyke, C.M., Michels, D.J., Moses, J.D., Socker, D.G., Derc, K.P., Lamy, P.L., Llebaria, A., Bout, M.V., Schwenn, R., Simnett, G.M., Bedford, D.K. and Eyles, C.J.: 1995, *Solar Phys.* **162**, 357.
Chae, J.: 2001, *Astrophys. J.* **560**, L95.
Chae, J., Wang, H., Qiu, J., Goode, P.R., Strous, L. and Yun, H.S.: 2001, *Astrophys. J.* **560**, 476.
Cliver, E.W. and Hudson, H.: 2002, *J. Atmos. Solar Ter. Phys.* **64**, I2, 231.
Delaboudiniere, J.-P., Artzner, G.E., Brunaud, J., Gabriel, A.H., Hochedez, J.F., Millier, F., Song, X.Y., Au, B., Dere, K.P., Howard, R.A., Kreplin, R., Michels, D.J., Moses, J.D., Defise, J.M.,

Jamar, C., Rochus, P., Chauvineau, J.P., Marioge, J.P., Catura, R.C., Lemen, J.R., Shing, L., Stern, R.A., Gurman, J.B., Neupert, W.M., Maucherat, A., Clette, F., Cugnon, P. and van Dessel, E.L.: 1995, *Solar Phys.* **162**, 291.

Démoulin, P. and Berger, M.A.: 2003, *Sol. Phys.* **215**, 203.

Démoulin, P., Mandrini, C.H., van Driel-Gesztelyi, L., Thompson, B.J., Plunkett, S., Kovári, Zs., Aulanier, G. and Young, A.: 2002, *Astron. Astrophys*. **382**, 650.

Démoulin, P., Mandrini, C.H., van Driel-Gesztelyi, L., López Fuentes, M. and Aulanier, G.: 2002b, *Solar Phys.* **207**, 87.

DeVore, C.R.: 2000, *Astrophys. J.* **539**, 944.

Dryer, M., Andrews, M.D., Aurass, H., DeForest, C., Galvin, A.B., Garcia, H., Ipavich, F.M., Karlicky, M., Kiplinger, A., Klassen, A., Meisner, R., Paswaters, S.E., Smith, Z., Tappin, S.J., Thompson, B.J., Watari, S.J., Michels, D.J., Brueckner, G.E., Howard, R.A., Koomen, M.J., Lamy, P., Mann, G., Arzner, K. and Schwenn, R.: 1998, *Solar Phys.* **181**, 159.

Emonet, T. and Moreno-Insertis, F.: 1998, *Astrophys. J.* **492**, 804.

Finn, J.H. and Antonsen, T.M.: 1985, *Comments Plasma Phys. Contr. Fusion* **9**, 111.

Green, L.M., Harra, L.K., Matthews, S.A. and Culhane, J.L.: 2001, *Solar Phys.* **200**, 189.

Green, L.M., López-Fuentes, M.C., Mandrini, C.H., Démoulin, P., van Driel-Gesztelyi, L. and Culhane, J.L.: 2002, *Solar Phys.* **208**, 43.

Hale, G.E.: 1925, *Pub. Astron. Soc. Pacific* **37**, 268.

Hale, G.E. and Nicholson, S.B.: 1925, *Astrophys. J.* **62**, 270.

Hale, G.E., Ellerman, F., Nicholson, S.B. and Joy, A.H.: 1919, *Astrophys. J.* **49**, 153.

Kusano, K., Maeshiro, T., Yokoyama, T. and Sakurai, T.: 2002, *Astrophys. J.* **577**, 501.

Lepping, R.P., Burlaga, L.F. and Jones, J.A.: 1990, *J. Geophys. Res.* **95**, 11957.

Lepping, R.P., Burlaga, L.F., Szabo, A., Ogilvie, K.W., Mish, W.H., Vassiliadis, D., Lazarus, A.J., Steinberg, J.T., Farrugia, C.J., Janoo, L. and Mariani, F.: 1997, *J. Geophys. Res.* **102**, 14049.

Longcope, D.W. and Welsch, B.T.: 2000, *Astrophys. J.* **545**, 1089.

López Fuentes, M., Démoulin, P., Mandrini, C.H. and van Driel-Gesztelyi, L.: 2000, *Astrophys. J.* **544**, 540.

López Fuentes, M., Démoulin, P., Mandrini, C.H. and van Driel-Gesztelyi, L.: 2003, *Astron. Astrophys.* **397**, 305.

Low, B.C.: 1996, *Solar Phys.* **167**, 217.

Maia, D., Vourlidas, A., Pick, M., Howard, R., Schwenn, R. and Magalhes, A.: 1999, *J. Geophys. Res.* **104**, 12507.

Mandrini, C.H., Démoulin, P., van Driel-Gesztelyi, L., Aulanier, G., Thompson, B.J., Plunkett, S. and Kővári, Zs.: 2001, in: G. Mathys, S.K. Solanki and D.T. Wickramasinghe (eds.), *ASP Conf. Ser.: Magnetic Fields Across the Hertzsprung-Russell Diagram* (*Vol.* 248) p. 139.

Mandrini, C.H., van Driel-Gesztelyi, L., Thompson, B.J., Plunkett, S., Démoulin, P. and Aulanier, G.: 2000, *Geofis. Inter.* **39**, 1, 73.

Marubashi, K.: 1997, in: N. Crooker, J.A. Joselyn and J. Feynman (eds.), *Coronal Mass Ejections*, Geophysical Monograph 99, American Geophysical Press, Washington DC, p. 147.

Moreno-Insertis, F. and Emonet, T.: 1996, *Astrophys. J.* **472**, L53.

Moon, Y.-J., Chae, J., Choe, G.S., Wang, H., Park, Y.D., Yun, H.S., Yurchyshyn, V. and Goode, P.R.: 2002, *Astrophys. J.* **574**, 1066.

Nindos, A. and Zhang, H.: 2002, *Astrophys. J.* **573**, L133.

Pevtsov, A.A. and Balasubramaniam, K.S.: 2003, *Adv. Space Res.* **32**, Vol. 10, 1867.

Richardson, I.G.: 1997, in: N. Crooker, J.A. Joselyn and J. Feynman (eds.), *Coronal Mass Ejections*, Geophysical Monograph 99, American Geophysical Press, Washington DC, p. 189.

Richardson, R.S.: 1941, *Astrophys. J.* **93**, 24.

Rust, D.M.: 1994, *Geophys. Res. Lett.* **21**, 241.

Scherrer, P.H., Bogart, R.S., Bush, R.I., Hoeksema, J.I., Kosovicher, A.G., Schov, J., Rosenberg, W., Springer, L., Tarbell, T.D., Title, A., Wolfson, C.J., Zayer, I. and MDI Engineering Team: 1995, *Solar Phys.* **162**, 129.

Shimazu, H. and Marubashi, K.: 2000, *J. Geophys. Res.* **105**, 2365.

Tsuneta, S., Acton, L., Bruner, M., Lemen, J., Brown, W., Caravalho, R., Catura, R., Freeland, S., Jurcevich, B. and Owens, J.: 1991, *Solar Phys.* **136**, 37.

van Driel-Gesztelyi: 1998, in: C.E. Alissandrakis and B. Schmieder (eds.), *ASP Conf. Ser., Second Advances in Solar Physics Euroconfences: Three-Demensional Structure of Soalr Active Regions* (*Vol.* 155) p. 202.

van Driel-Gesztelyi, L., Démoulin, P. and Mandrini, C.H.: 2003a, *Adv. Space Res.* **32**, (Vol. 10) p. 1855.

van Driel-Gesztelyi, L., Mandrini, C.H., Thompson, B.J., Plunkett, S., Aulanier, G., Démoulin, P., Schmieder, B. and DeForest, C.: 1999, in: B. Schmieder, A. Hofmann and J. Staude (eds.), *ASP Conf. Ser.: Magnetic Fields and Oscillations* (*Vol*. 184) p. 302.

van Driel-Gesztelyi, L., Mandrini, C.H., Démoulin, P.: 2003b, in: J.-C. Hénoux and C. Fang (eds.), *Second Franco-Chinese Meeting on Solar Physics: Understanding Active Phenomena, Progress and Perspectives*, World Publishing Corporation, **37**.

Webb, D.F., Cliver, E.W., Crooker, N.U., St. Cry, O.C. and Thompson, B.J.: 2000, *J. Geophys. Res.* **105**, 7491.

Yurchyshyn, V.B., Wang, H., Goode, P.R. and Deng, Y.: 2001, *Astrophys. J.* **563**, 381.

Zhao, X.P., Hoeksema, J.T. and Marubashi, K.: 2001, *J. Geophys. Res.* **106**, 15643.